
RESOLVING THE BAND ALIGNMENT OF INAS/INASSB MID-WAVE-INFRARED TYPE-II SUPERLATTICES

Michał Rygała

Wrocław University of Science and Technology
michal.rygala@pwr.edu.pl

Julian Zanon

Eindhoven University of Technology

Andreas Bader

Julius-Maximilians-Universität Würzburg

Tristan Smołka

Wrocław University of Science and Technology

Fabian Hartmann

Julius-Maximilians-Universität Würzburg

Sven Höfling

Julius-Maximilians-Universität Würzburg

Michael E. Flatté

University of Iowa
Eindhoven University of Technology

Marcin Motyka

Wrocław University of Science and Technology

ABSTRACT

In this work, three InAs/InAs_{0.65}Sb_{0.35} superlattices with different periods were investigated using photoluminescence and photoreflectance measurements and their band structure was simulated using a 14 bulk-band $\mathbf{k}\cdot\mathbf{p}$ model. The structures were studied by analyzing the evolution of the spectral features in temperature and excitation power to determine the origin of optical transitions. After identifying which of these are related to the superlattice mini-bands, a rich collection of observed higher-order optical transitions was compared with refractive-index calculations. This procedure was used to adjust the parameters of the theoretical model, namely the bowing parameters of the InAsSb valence band offset and bandgap. It was also shown that the spectroscopy of the higher-order states combined with numerical modeling of the refractive index is a powerful tool for improvement of the material parameters, presenting a new approach to material studies of advanced semiconductor heterostructures.

1 INTRODUCTION

In the last 60 years of searching for an efficient infrared detector, many solutions were reported, with their own advantages and disadvantages. The recent development of highly efficient growth procedures for $A^{III}B^V$ semiconductor alloys [1, 2] is closing the technological gap between detectors based on low-dimensional structures and widely used HgCdTe alloys. [3, 4, 5, 6, 7, 8] Despite the overall lower quantum efficiency of $A^{III}B^V$ semiconductor-based detectors in comparison to $A^{II}B^{VI}$, they are more mechanically stable due to the covalent bonding of the atoms [9] and are generally less hazardous to health and the environment. [10, 11, 12]

Primary interest has focused on two material systems with type-II superlattice (T2SL) architecture - InAs/GaSb and InAs/InAsSb. Both of these materials were widely investigated, with overall optical properties favoring the InAs/GaSb SLs and electronic properties favoring the InAs/InAsSb SLs. [13, 14] The absorption coefficient of the "Ga-free" SLs is lower, mainly due to the unfavorable overlap of the electron and hole states within the structure. [15, 16] However, they exhibit much longer Shockley-Read-Hall (SRH) carrier lifetimes than their Ga-containing counterparts [17, 18, 19, 20, 21, 22], which has been attributed to the removal of gallium from the structure. [23] The detectivity of the InAs/InAsSb-based detectors influenced by both of these effects has been reported to be approaching the ultimate

efficiency reported for the HgCdTe and defined by semi-empirical curves, such as "Rule-07", "Law 19", or "Rule-22". [8]

In InAs/InAsSb alloys the energy difference between the bottom of the valence and conduction bands can be modified by the composition of the InAsSb layer and the thickness of the single superlattice period. The lattice constant of the alloy follows Vegard's law, therefore it varies linearly with the composition, whereas the approximation of the bandgap uses an additional bowing parameter. [24] Moreover, to fully describe the transition energies between the confined states within the InAs/InAsSb T2SL it is crucial to know the energy difference between the bottoms of the valence bands of InAsSb and InAs. This is usually described by the valence band offset parameter (VBO), which has been presented to be composition-dependent [25] but also temperature-dependent [26, 27], leading to a plethora of speculations in terms of the InAsSb valence band position and its bandgap. It has also been shown that the type of band discontinuity can vary between type I, IIa, IIb, and III (broken gap alignment) [18].

In this work, we present the results of the experimental and numerical investigation of InAs/InAs_{0.65}Sb_{0.35} T2SLs on a GaSb substrate with different period lengths. The analysis of the optical response of the structures was performed using a 14 bulk band $\mathbf{k}\cdot\mathbf{p}$ model to perform calculations of confined states. The InAsSb VBO and bandgap bowing parameters were modified during model optimization in order to match the results of refractive index calculations in the presence of external carriers and photomodulated reflectance (PR) spectra.

2 MATERIALS AND METHODS

2.1 Sample growth

Investigated samples consisted of InAs/InAs_{0.65}Sb_{0.35} superlattices with varying periods P of 5, 6 and 8 nm. The structures were grown using molecular beam epitaxy on n-type doped GaSb:Te substrates with doping concentration of 10¹⁸ cm⁻³. Growth was initiated with a deoxidization step at 560 °C which was followed by the growth of an undoped 200 nm GaSb buffer layer at a substrate temperature of 500 °C. Subsequently, the growth temperature was reduced to 430 °C for the growth of the T2SL. The thicknesses of the individual SL layers were chosen to achieve overall strain compensation on the GaSb substrate, therefore making the system lattice-matched. For the $P = 5$ nm sample, the InAs and InAsSb thicknesses were 3.71 and 1.23 nm, respectively. For $P = 6$ nm, the layer thicknesses were 4.45 (InAs) and 1.55 nm (InAsSb), and for $P = 8$ nm: 5.94 (InAs) and 2.06 nm (InAsSb). 100 ($P = 8, 6$ nm) or 150 ($P = 5$ nm) periods of the SLs were grown and the structures capped with a 50 nm undoped GaSb layer.

2.2 Fourier spectroscopy

Photoluminescence (PL) and photoreflectance (PR) measurements were performed on a Vertex 80v Fourier spectrometer using a 660 nm excitation beam. The samples were kept in a liquid helium cryostat at a stable 10 K temperature. The emitted or reflected light was collected by an MCT detector in a step scan measurement mode correlated with a chopper by a homodyne for a 300 ms integration time per interferometer mirror step. This experimental setup has proven useful for investigating weak transitions in semiconductor nanostructures designed for the infrared spectral region. [28, 29, 30, 31]

2.3 Numerical model

In order to obtain the VBO between the InAs and InAsSb layers, the photoreflectance spectra for the three samples with different periods were compared with the change in the refractive index (i.e., Δn) calculated using the 14 bulk band $\mathbf{k}\cdot\mathbf{p}$ model from QuantCAD's software called CADtronics [32].

The 14 bulk band $\mathbf{k}\cdot\mathbf{p}$ model includes in its basis two antibonding s states, six valence bonding p states, and six antibonding p states. The inclusion of these states takes into account the inversion asymmetry present in zincblende materials (such as InAs or InSb), and provides a more accurate treatment for the heavy-hole band mass [33] as the momentum \mathbf{k} is further away from $\mathbf{k}=0$. Furthermore, the model used here also considers energy shifts due to lattice-mismatch strain between the two different semiconductors.

The VBO is obtained after an optimization procedure, where the transitions obtained in Δn are compared to the ones from the photoreflectance. As detailed in [Supplementary Materials](#), the refractive index $n(E; \rho)$ for a given carrier density ρ is calculated as a function of energy E using the absorption $\alpha(E; \rho)$, calculated using the complex dielectric function $\epsilon(E)$. Following that, the change in the refractive index Δn is obtained with $\Delta n = n(E; 0) - n(E; \rho)$. While comparing the transitions energies between the photoreflectance and Δn , a careful analysis is carried out considering different values for the valence band bowing b_v and the gamma gap bowing b_g from the InAsSb layer. b_v and b_g are

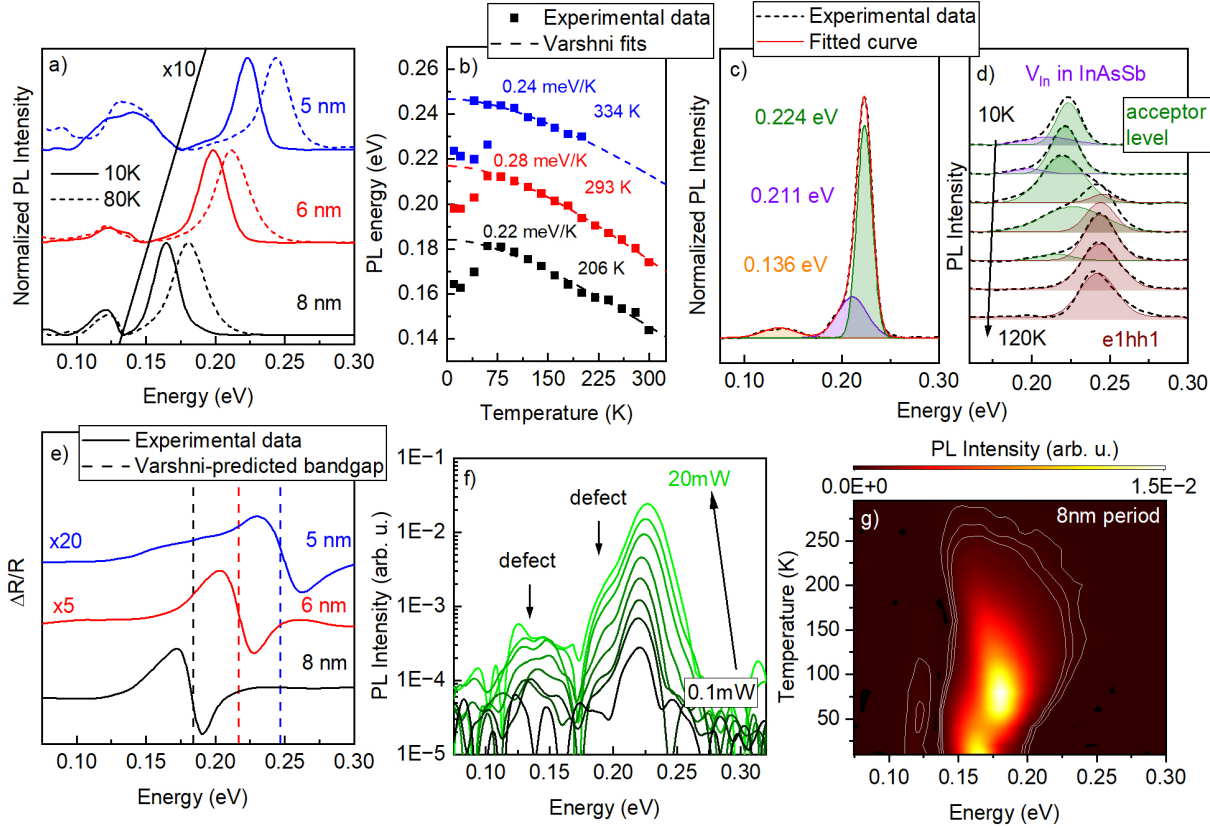


Figure 1: Optical properties of the InAs/InAs_{0.65}Sb_{0.35} superlattices. a) Normalized photoluminescence spectra of the samples at 10 K (solid line) and 80 K (dashed line) temperature shown in blue, red and black for sample with 5 nm, 6 nm and 8 nm period, respectively. b) Energies of the dominating photoluminescence emission fitted with Varshni equation shown in blue, red and black for samples with 5 nm, 6 nm and 8 nm period, respectively, with the parameters of the fitted function - α and β . c) Close up of the emission lineshape of 5 nm period sample at 10 K temperature with the red fitted curve comprising of three distinct gaussian peaks with the green, violet and orange colours representing the optical transitions originating from acceptor level, a defect state corresponding to indium vacancy and an unknown confined state. d) Temperature evolution of the photoluminescence signal from the sample with 5 nm period with fitted gaussian peaks colour coded as in the panel c and additional wine colour representing a fundamental transition from the first confined states within the conduction mini-band to the valence mini-band. e) Photoreflectance spectra of the fundamental transitions shown in blue, red and black for the samples with 5 nm, 6 nm and 8 nm period, respectively, with the bandgap energies predicted by fitting the Varshni equation to higher-temperature energies of the dominating photoluminescence emission, presented as dashed lines with colours corresponding to the samples. f) Power-dependent photoluminescence spectra of the sample with 5 nm period at 10 K in logarithmic scale, denoting the defect states within the spectra. g) Temperature evolution of photoluminescence signal from 8 nm period sample showing the maximum of signal intensity at around 80 K.

related to the valence band E_v and gap E_g energies of the InAsSb layer at the gamma point, as presented in Eq.(1).

$$E_{v(g)}(\text{InAs}_{1-x}\text{Sb}_x) = (1-x)E_{v(g)}(\text{InAs}) + xE_{v(g)}(\text{InSb}) - b_{v(g)}x(1-x) \quad (1)$$

3 RESULTS

The optical properties of the samples are presented in Figure 1. All samples exhibit a shift of the emission to higher energies caused by changing the temperature from 10 to 80 K, as shown in Figure 1a. The energy of the main photoluminescence signal also slightly deteriorates at temperatures below 80 K from the bandgap, predicted by fitting the energies of high-temperature range emission with the Varshni equation, as shown in Figure 1b. The non-monotonic

behavior of the emission energy in varying temperature referred to as "S-shape" has been previously investigated and attributed to carrier localization due to mid-gap trap states.[34, 35] The fitting procedure of high-temperature side yielded the values of parameters α and β in the range of 0.22 – 0.28 meV/K and 206 – 334 K, respectively. While the α parameter is in agreement with the values reported in literature [34, 36, 37, 35], the β is slightly higher, possibly due to the lack of emission data from the fundamental transition in low temperature regime. The bandgap energies predicted by the fitting were equal to 0.246, 0.217 and 0.185 eV for 5, 6 and 8 nm period sample, respectively.

To further explore this unusual behavior, we performed a detailed analysis of emission lineshape which was shown for 5 nm period sample in Figure 1c. At 10 K, it is possible to distinguish three separate signals comprising the photoluminescence envelope at energies 0.224, 0.211 and 0.136 eV. After the temperature of the sample was increased to 40 K, another signal (presented in wine color in the Figure 1d) emerged at a higher energy corresponding to the $e1hh1$ energy predicted by the Varshni equation. It later dominates the photoluminescence spectra at the cost of the signal denoted in green colour. By comparing these findings with literature [38, 39] we identified the green signal as an acceptor level-related transition, while the violet is predicted to arise from a mid-gap trap level related to an indium vacancy in InAsSb layer of the superlattice. This type of structural defect is predicted to be one of the main limitations in terms of efficiency of InAsSb-based infrared detectors. [21]

The defect-related origin of the dominant signal at 10 K is also supported by photoreflectance measurements as presented in Figure 1e. The resonance energies of the photoreflectance spectra match the predicted low-temperature bandgap energies obtained from the Varshni equation. The main low-temperature emission must therefore arise from a bound level characterized by low density of states, which would not be observable through absorption-based experiments. These findings were also supported by power-dependent photoluminescence measurements shown in Figure 1f. The power dependence of the main low-temperature emission peak is sub-linear which indicates that the emission is caused by carrier recombination to a confined (defect) state or related to donor-acceptor levels. Increasing the temperature to 77 K resulted in a linear relation between excitation power and photoluminescence intensity, expected for high-intensity regime excitation of type-II quantum system. [40, 41, 42] Defect-related emission at lower energies was also investigated and it resulted in an exponent value close to 1/2 that is characteristic for a bound-to-defect optical transitions. [43] The value remained constant for 77 K, which indicates a high activation energy of this defect. Further study of the relation between the emission and the temperature of the sample as presented in Figure 1g provides more information about the origin of the emission. The intensity is highest at a temperature in which the energy of the transition is in agreement with the Varshni-predicted bandgap. The defect-related emission is observable up to 150 K.

The photoreflectance response of the 8 and 6 nm samples for a broader range of energy are presented in Figure 2 (panel a and b, respectively). Apart from the fundamental optical transitions at 0.180 eV (8nm sample) and 0.216 eV (6 nm sample), there are other features corresponding to higher-order states within the superlattice. The sample with a 5 nm period also exhibited higher-order features and is presented in the later parts of the manuscript. The resonances of the reflectivity spectra were fitted with the function described by the equation:

$$\frac{\Delta R}{R} = Re \sum_{j=1}^n [C_j^{i\theta_j} (E - E_j + i\Gamma_j)]^{-m_j} \quad (2)$$

where n is the number of optical transitions, C_j and θ_j are amplitude and phase parameters, E_j and Γ_j are energy and broadening of the transition and m_j describes the lineshape of the modulation accounting for the type of transition (excitonic, free-carrier, etc.)[44]. For clarity of presentation, the transitions were also shown as moduli in Figure 2 (panels c and d) described by the equation:

$$\sigma = \frac{|C|}{[(E - E_0)^2 + \Gamma^2]^{\frac{m}{2}}} \quad (3)$$

To gain insight into the origin of these higher energy states and at which point of superlattice band structure these transitions occur, we compared the photoreflectance spectra with the calculated refractive index curves. The curves were simulated for several different values of VBO obtained by varying the bowing parameters of InAsSb valence band offset b_v and band gap b_g with the results shown in Figure 3 on panels a) and b). We compared the transition energy obtained from the refractive index calculations with the photoreflectance by introducing the parameter $\Delta = \Delta_1 + \Delta_2 + \Delta_3$, with Δ_i describing the difference in energies obtained between the refractive index and the photoreflectance for the i^{th} ($=1,2,3$) transition. The transition energy from the photoreflectance is extracted using Eq. (3) as shown in Figure 2, while in the refractive index the energy transition is defined as the middle point between the maximum and minimum resonance energies (equivalent to the maximum value picked by the change in the absorption $\Delta\alpha = \alpha(E; 0) - \alpha(E; \rho)$). All the results in Figures 3 and 4 assume layer thicknesses and Sb composition (35%) for the superlattice as expected during an ideal growth procedure. In the [Supplementary Material](#), we presented additional analysis for the refractive index taking into account certain imperfections during growth, e.g., slightly different layer thicknesses and Sb composition deviating from the nominal values.

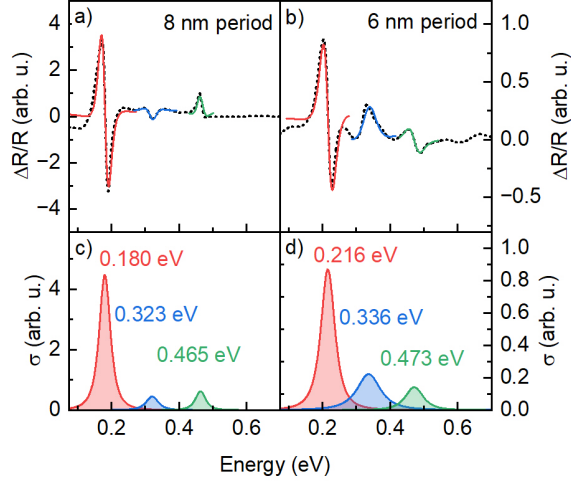


Figure 2: Results of the photoreflectance experiment. a,b) Photoreflectance spectra of the sample with 8 nm (panel a)), and 6 nm (panel b) period at 10 K temperature with fitted curves using Equation 2. c,d) Moduli calculated with the Equation 3 using the parameters from the fitting procedure of the photoreflectance response for sample with 8 nm (panel c)) and 6 nm period (panel d)).

The inclusion of optical transitions beyond the band gap with Δ shows a clear advantage in defining the VBO between the InAs and InAsSb layers. By comparing Figures 3a and 3b, it becomes clear that it is possible to minimize Δ with a set of bowing parameters resulting in a specific VBO and band gap, while for Δ_1 the VBO and band gap bowing parameters seem mutually dependent with multiple sets yielding near 0 meV values. Table 1 shows a summary of the smallest values for Δ and Δ_1 , including the results for the 6 nm and 5 nm period superlattices. Among all superlattices in Table 1, the 8 nm period has the smallest value for Δ as a result of its second and third resonances in the photoreflectance having a better resolution, when compared to the results for 6 and 5 nm period samples, as shown in Figure 3e. The lower resolution of resonances for 6 and 5 nm samples caused Δ minima to broaden to a range defined by $b_v = [-0.65 \text{ eV}, -0.45 \text{ eV}]$ and $b_g = [0.8 \text{ eV}, 1 \text{ eV}]$ which was shown in [Supplementary Material](#). Using the optimal values of b_v and b_g from Table 1 for all the samples the calculated refractive index curves match the optical features in the photoreflectance spectra as shown in Figure 3c.

Table 1: Results obtained for VBO, b_v and b_g after optimization in Figure 3a). The 6 and 5 nm superlattice periods have their values for Δ and Δ_1 obtained with the same optimal parameters found for the 8 nm superlattice period.

Period	Δ (meV)	Δ_1 (meV)	VBO (meV)	b_v (eV)	E_g (meV)	b_g (eV)
8 nm	6	1				
6 nm	34	2	328	-0.6	168	0.8
5 nm	40	5				

In Figure 3e the optimal bowing parameters, $b_v = -0.6 \text{ eV}$ and $b_g = 0.8 \text{ eV}$, are compared to those in refs. [25, 27]. This is done by calculating the valence-band energy E_v and band-gap energy E_g at the gamma point as a function of the Sb composition (%) for the InAsSb layer, using Eq.(1). Note that, E_v is referenced to the valence-band edge of InSb. For Sb = 35%, our parameters result in $E_v = 416 \text{ meV}$ and $E_g = 168 \text{ meV}$. Comparing these results with those obtained with Vurgaftaman's parameters [25], E_v is 137 meV larger and E_g is 32 meV smaller, respectively; Compared to T. Manyk's [27], which are based on an experimental study of superlattices with various Sb content [24], E_v is 30 meV larger and E_g is 21 meV smaller.

In order to identify the originating states resulting in photoreflectance resonances in Figure 3c, we plotted the change in the absorption $\Delta\alpha \equiv \alpha(E; 0) - \alpha(E; \rho)$ with the band structure, as shown in Figure 4. Three panels on Figure 4a clearly show that the transitions assigned by, respectively, $\text{HH}_1 \rightarrow \text{CB}_1$, $\text{LH}_1 \rightarrow \text{CB}_1$ and $\text{HH}_3 \rightarrow \text{CB}_1$, occur predominantly close to $k_z = 0$. For 8 nm period the third resonance for Δn in Figure 4d has a small additional contribution from the

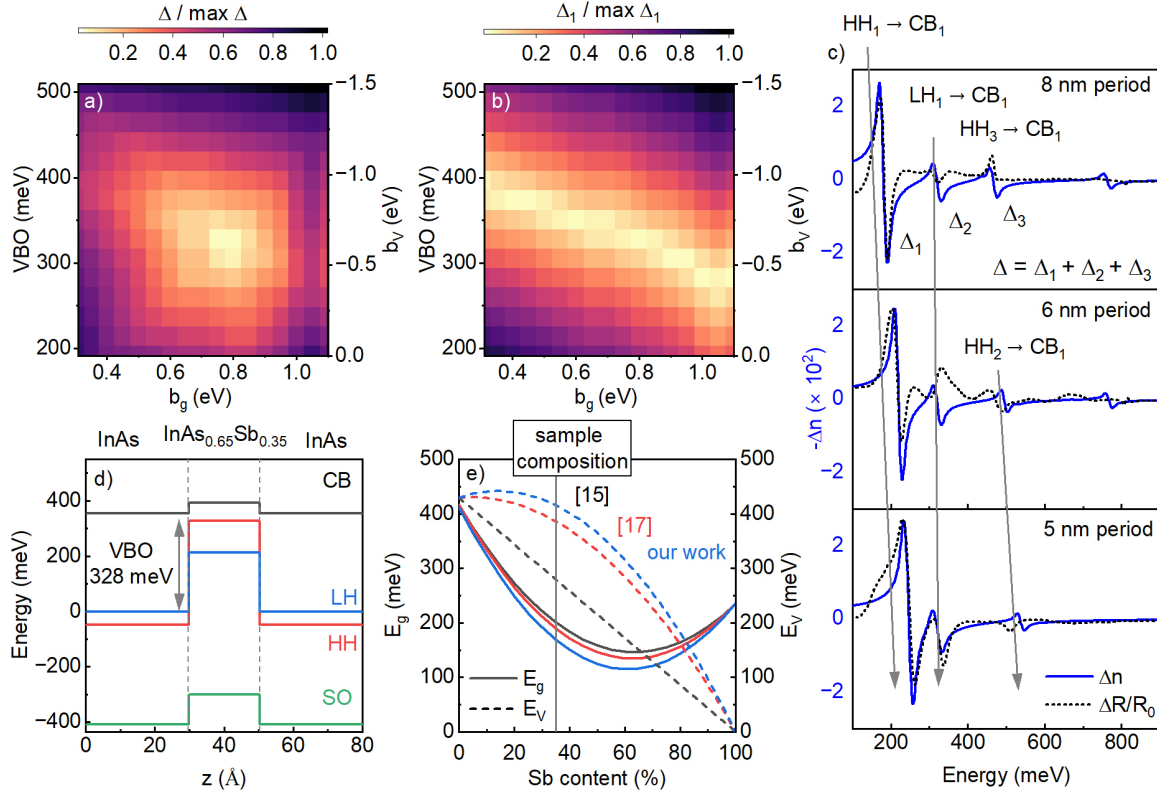


Figure 3: Comparison between the numerical calculations from $14 \times 14 \mathbf{k} \cdot \mathbf{p}$ model and the results of photoreflectance measurements. a,b) Optimization maps for Δ (panel a) and Δ_1 (panel b) for the 8 nm superlattice period made by plotting the difference between the resonant energies from the calculated refractive index Δn and the energies obtained from the photoreflectance spectra $\Delta R/R$. $\Delta n = n(E; 0) - n(E; \rho)$ was calculated for a given combination of InAsSb valence band offset b_v and gamma gap b_g bowing parameters, assuming a photoexcited carrier density ρ equal to $2 \times 10^{16} \text{ cm}^{-3}$. c) Comparison between Δn , calculated with the optimal parameters found in a), i.e., $b_v = -0.6 \text{ eV}$ and $b_g = 0.8 \text{ eV}$, and $\Delta R/R$ for different superlattices periods P . Each set of parameters $\{b_g, b_v\}$ provides a valence band offset (VBO) as shown in panel d) with the conduction (CB), heavy-hole (HH), light-hole (LH) and split-off (SO) band edges. e) Composition dependent Eq.(1) for the optimal bowing parameters obtained in this work ($b_v = -0.6 \text{ eV}$ and $b_g = 0.8 \text{ eV}$), and parameters reported in the literature (Vurgaftman *et al.* [25] $b_v = 0 \text{ eV}$ and $b_g = 0.67 \text{ eV}$; Manyk *et al.* [27] $b_v = -0.47 \text{ eV}$ and $b_g = 0.72 \text{ eV}$).

transition $\text{HH}_2 \rightarrow \text{CB}_1$. This transition has the highest contribution to the third resonance for 6 and 5 nm periods. The corresponding figures for the remaining samples were shown in the [Supplementary Material](#).

4 CONCLUSION

In this work, three InAs/InAs_{0.65}Sb_{0.35} superlattices with different periods were investigated using photoluminescence and photoreflectance measurements. The photoluminescence from 80 K to 10 K shows an unexpected progression for the emission energy for all the samples that is not in agreement with the Varshni-predicted bandgap. We attribute this behavior to localized states, such as traps caused by indium vacancies. This hypothesis is supported by the photoreflectance data, showing that its main resonance happens at the energy expected to be the bandgap for the superlattice.

The photoreflectance is further compared with the change in refractive index, which is calculated using a $14 \times 14 \mathbf{k} \cdot \mathbf{p}$ model for various InAsSb bowing parameters of the valence band offset, b_v , and the bandgap b_g . We identify the bands in the superlattices associated with the transitions in the photoreflectance, and show that higher-energy optical transitions (beyond the fundamental band-gap transition) strongly impact the choice of the valence band offset between

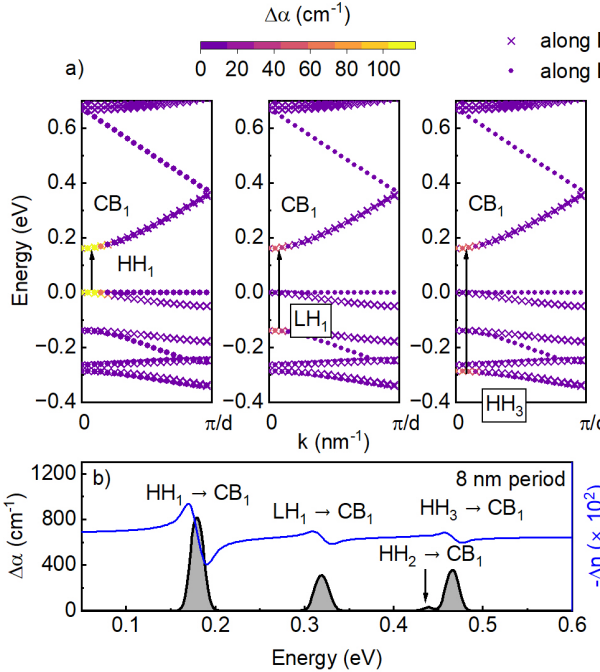


Figure 4: a) Band structure for the 8 nm period superlattice with the absorption $\Delta\alpha \equiv \alpha(E; 0) - \alpha(E; \rho)$ resolved in the k -space. d represents the superlattice period. b) Calculated refractive index Δn in the presence of external carriers with a density $\rho = 2 \times 10^{16} \text{ cm}^{-3}$, plotted with a sum of $\Delta\alpha$ corresponding to the states with the highest contribution to the optical resonances. k_z and k_{\parallel} refer to directions along and perpendicular (i.e., parallel to the layer plane) to the growth direction z , respectively. The remaining superlattice periods were presented in [Supplementary material](#).

InAs and InAsSb. Our comparison yields a InAs_{0.65}Sb_{0.35} valence band offset (in relation to InAs) of 328 meV, obtained using the bowing parameters $b_v = -0.6$ eV and $b_g = 0.8$ eV.

ACKNOWLEDGEMENTS

This work has been funded by the German Federal Ministry of Research, Technology, and Space (BMFTR) within the joint research project RIBKD (13N16964). J. Z. was financially supported by Marie Skłodowska-Curie Grant No. 956548.

SUPPLEMENTARY MATERIALS

See [Supplementary Material](#) for more information on the mathematical formulas used for calculations of the refractive index, extended optimization study taking into account the imperfections of the growth procedure and the results of the optimization for the superlattices with 6 and 5 nm period.

DATA SHARING POLICY

The data that support the findings of this study are available from the corresponding author upon reasonable request.

References

- [1] A. Rogalski. History of infrared detectors. *Opto-Electronics Review*, 20(3):279–308, 2012.
- [2] A. Rogalski and P. Martyniuk. Inas/gainsb superlattices as a promising material system for third generation infrared detectors. *Infrared Physics & Technology*, 48(1):39–52, 2006.

- [3] D. L. Smith and C. Mailhiot. Proposal for strained type ii superlattice infrared detectors. *Journal of Applied Physics*, 62(6):2545–2548, 1987.
- [4] R. Rehm, M. Walther, F. Fuchs, J. Schmitz, and J. Fleissner. Passivation of inas/(gain)sb short-period superlattice photodiodes with 10um cutoff wavelength by epitaxial overgrowth with alxga1-xasysb1-y. *Applied Physics Letters*, 86(17):173501, 2005.
- [5] S. Maimon and G. W. Wicks. nbn detector, an infrared detector with reduced dark current and higher operating temperature. *Applied Physics Letters*, 89(15):151109, 2006.
- [6] E. Plis, S-J. Lee, Z. Zhu, A. Amtout, and S. Krishna. Inas/gasb superlattice detectors operating at room temperature. *IEEE Journal of Selected Topics in Quantum Electronics*, 12(6):1269–1274, 2006.
- [7] B-M. Nguyen, D. Hoffman, E. K. Huang, P-Y. Delaunay, and M. Razeghi. Background limited long wavelength infrared type-ii inas/gasb superlattice photodiodes operating at 110k. *Applied Physics Letters*, 93(12):123502, 2008.
- [8] M. Kopytko, P. Madejczyk, K. Murawski, Ł. Kubiszyn, K. Michalczewski, B. Seredyński, K. Szlachetko, J. Jureńczyk, W. Gawron, and J. Rutkowski. Comparison of type II superlattice InAs/InAsSb barrier detectors operating in the mid-wave infrared range. *Journal of Applied Physics*, 136(1):014501, 2024.
- [9] A. Rogalski, P. Martyniuk, and M. Kopytko. InAs/GaSb type-II superlattice infrared detectors: Future prospect. *Applied Physics Reviews*, 4(3):031304, 2017.
- [10] Imtiaz Madni. *Characterization of MBE-grown HgCdTe and related II-VI materials for next generation infrared detectors*. PhD thesis, The University of Western Australia, 2017.
- [11] M. Kopytko and A. Rogalski. Performance evaluation of type-ii superlattice devices relative to hgcdte photodiodes. *IEEE Transactions on Electron Devices*, 69(6):2992–3002, 2022.
- [12] L. Nordin, A. J. Muhowski, and D. Wasserman. High operating temperature plasmonic infrared detectors. *Applied Physics Letters*, 120(10):101103, 2022.
- [13] A. Rogalski, P. Martyniuk, M. Kopytko, P. Madejczyk, and S. Krishna. InAsSb-based infrared photodetectors: Thirty years later on. *Sensors*, 20(24):7047, 2020.
- [14] Dhafer O. Alshahrani, M. Kesaria, Ezekiel A. Anyebe, V. Srivastava, and Diana L. Huffaker. Emerging Type-II superlattices of InAs/InAsSb and InAs/GaSb for mid-wavelength infrared photodetectors. *Advanced Photonics Research*, 3(2):2100094, 2022.
- [15] C. Mailhiot and D. L. Smith. Long-wavelength infrared detectors based on strained inas-ga1-xinxsb type-ii superlattices. *Journal of Vacuum Science & Technology A*, 7(2):445–449, 1989.
- [16] D. L. Smith and C. Mailhiot. Theory of semiconductor superlattice electronic structure. *Rev. Mod. Phys.*, 62:173–234, 1990.
- [17] G. Belenky, D. Donetsky, G. Kipshidze, D. Wang, L. Shterengas, W. L. Sarney, and S. P. Svensson. Properties of unrelaxed $\text{InAs}_{1-x}\text{Sb}_x$ alloys grown on compositionally graded buffers. *Applied Physics Letters*, 99(14):141116, 2011.
- [18] E. H. Steenbergen, B. C. Connelly, G. D. Metcalfe, H. Shen, M. Wraback, D. Lubyshev, Y. Qiu, J. M. Fastenau, A. W. K. Liu, S. Elhamri, O. O. Cellek, and Y.-H. Zhang. Significantly improved minority carrier lifetime observed in a long-wavelength infrared III-V type-II superlattice comprised of InAs/InAsSb. *Applied Physics Letters*, 99(25):251110, 2011.
- [19] B. V. Olson, E. A. Shaner, J. K. Kim, J. F. Klem, S. D. Hawkins, L. M. Murray, J. P. Prineas, M. E. Flatté, and T. F. Boggess. Time-resolved optical measurements of minority carrier recombination in a mid-wave infrared InAsSb alloy and InAs/InAsSb superlattice. *Applied Physics Letters*, 101(9):092109, 2012.
- [20] Z.-Y. Lin, S. Liu, E. H. Steenbergen, and Y.-H. Zhang. Influence of carrier localization on minority carrier lifetime in InAs/InAsSb type-II superlattices. *Applied Physics Letters*, 107(20):201107, 2015.
- [21] Y. Aytac, B. V. Olson, J. K. Kim, E. A. Shaner, S. D. Hawkins, J. F. Klem, M. E. Flatté, and T. F. Boggess. Evidence of a Shockley-Read-Hall Defect State Independent of Band-Edge Energy in InAs/In(As, Sb) Type-II Superlattices. *Phys. Rev. Appl.*, 5:054016, 2016.
- [22] R. E. DeWames, J. Schuster, E. A. DeCuir Jr., and N. K. Dhar. Recombination processes in InAs/InAsSb type II strained layer superlattice MWIR nBn detectors. In Bjørn F. Andresen, Gabor F. Fulop, and Charles M. Hanson, editors, *Infrared Technology and Applications XLV*, volume 11002, page 110020W. International Society for Optics and Photonics, SPIE, 2019.

- [23] A. Józwikowska, M. Suligowski, and K. Józwikowski. Enhanced numerical design of two-barrier infrared detectors with III–V compounds heterostructures considering the influence of lattice strain and misfit dislocations on the band gap. *Optical and Quantum Electronics*, 51(7), 2019.
- [24] S. P. Svensson, W. L. Sarney, H. Hier, Y. Lin, D. Wang, D. Donetsky, L. Shterengas, G. Kipshidze, and G. Belenky. Band gap of $\text{InAs}_{1-x}\text{Sb}_x$ with native lattice constant. *Phys. Rev. B*, 86:245205, 2012.
- [25] I. Vurgaftman, J. R. Meyer, and L. R. Ram-Mohan. Band parameters for III–V compound semiconductors and their alloys. *Journal of Applied Physics*, 89(11):5815–5875, 2001.
- [26] Elizabeth Steenbergen. *Strain-balanced InAs-InAsSb Type-II Superlattices on GaSb Substrates for Infrared Photodetector Applications*. PhD thesis, Arizona State University, 2012.
- [27] T. Manyk, K. Michalczewski, K. Murawski, K. Grodecki, J. Rutkowski, and P. Martyniuk. Electronic band structure of InAs/InAsSb type-II superlattice for HOT LWIR detectors. *Results in Physics*, 11:1119–1123, 2018.
- [28] M. Rygała, J. Ziembicki, T. Smołka, A. Bader, G. Knebl, A. Pfenning, K. Ryczko, F. Hartmann, P. Scharoch, G. Sęk, S. Höfling, and M. Motyka. High optical anisotropy of the $\text{GaSb}/\text{Ga}_x\text{In}_{1-x}\text{As}_y\text{Sb}_{1-y}$ interface. *Phys. Rev. Appl.*, 23:014058, 2025.
- [29] M. Rygała, K. Ryczko, T. Smołka, D. Kujawa, P. Martyniuk, T. J. Ronningen, S. Krishna, and M. Motyka. Investigating the physics of higher-order optical transitions in InAs/GaSb superlattices. *Phys. Rev. B*, 104:085410, 2021.
- [30] M. Motyka and J. Misiewicz. Fast differential reflectance spectroscopy of semiconductor structures for infrared applications by using fourier transform spectrometer. *Applied Physics Express*, 3(11):112401, 2010.
- [31] M. Motyka, G. Sęk, F. Janiak, J. Misiewicz, K. Kłos, and J. Piotrowski. Fourier-transformed photoreflectance and fast differential reflectance of hgcdte layers. the issues of spectral resolution and fabry–perot oscillations. *Measurement Science and Technology*, 22(12):125601, 2011.
- [32] Wayne H Lau, JT Olesberg, and Michael E Flatte. Electronic structures and electron spin decoherence in (001)-grown layered zincblende semiconductors. *arXiv preprint cond-mat/0406201*, 2004.
- [33] Anthony Krier. *Mid-infrared semiconductor optoelectronics*, volume 118. Springer, 2007.
- [34] E.H. Steenbergen, J.A. Massengale, G. Ariyawansa, and Y.-H. Zhang. Evidence of carrier localization in photoluminescence spectroscopy studies of mid-wavelength infrared $\text{InAs/InAs}_{1-x}\text{Sb}_x$ type-II superlattices. *Journal of Luminescence*, 178:451–456, 2016.
- [35] K. Murawski, T. Manyk, and M. Kopytko. Analysis of temperature-dependent photoluminescence spectra in mid-wavelength infrared InAs/InAsSb type-II superlattice. *Journal of Electronic Materials*, 52:7089–7094, 2023.
- [36] T. Manyk, K. Michalczewski, K. Murawski, P. Martyniuk, and J. Rutkowski. InAs/InAsSb strain-balanced superlattices for longwave infrared detectors. *Sensors*, 19(8), 2019.
- [37] T. Smołka, M. Motyka, V. V. Romanov, and K. D. Moiseev. Photoluminescence spectroscopy of the InAsSb-based p-i-n heterostructure. *Materials*, 15(4), 2022.
- [38] K. Murawski, K. Majkowycz, T. Manyk, and M. Kopytko. Trap levels analysis in MWIR InAs/InAsSb T2SL photodiode. *Materials Science and Engineering: B*, 300:117112, 2024.
- [39] S. Krishnamurthy and Zhi Gang Yu. Green’s function-based defect identification in $\text{InAs/InAs}_{1-x}\text{Sb}_x$ strained layer superlattices. *AIP Advances*, 7(6):065310, 2017.
- [40] Y. S. Chiu, M. H. Ya, W. S. Su, and Y. F. Chen. Properties of photoluminescence in type-II GaAsSb/GaAs multiple quantum wells. *Journal of Applied Physics*, 92(10):5810–5813, 2002.
- [41] D. Alshahrani, M. Kesaria, Juan J Jiménez, D. Kwan, V. Srivastava, M. Delmas, F. M Morales, Baolai Liang, and Diana Huffaker. Effect of interfacial schemes on the optical and structural properties of InAs/GaSb Type-II superlattices. *ACS Applied Materials & Interfaces*, 15:8624–8635, 2023. doi: 10.1021/acsami.2c19292.
- [42] E. Rogowicz, J. Kopaczek, M. P. Polak, O. Delorme, L. Cerutti, E. Tournié, J.-B. Rodriguez, R. Kudrawiec, and M. Syperek. Carrier dynamics in $(\text{Ga,In})(\text{Sb,Bi})/\text{GaSb}$ quantum wells for laser applications in the mid-infrared spectral range. *Scientific Reports*, 12:12961, 2022.
- [43] Z. Deng, D. Guo, C. González Burguete, Z. Xie, J. Huang, H. Liu, J. Wu, and B. Chen. Demonstration of Si based InAs/GaSb type-II superlattice p-i-n photodetector. *Infrared Physics & Technology*, 101:133–137, 2019.
- [44] B. V. Shanabrook, O. J. Glembotck, and W. T. Beard. Photoreflectance modulation mechanisms in $\text{GaAs/Al}_x\text{Ga}_{1-x}\text{As}$ multiple quantum wells. *Phys. Rev. B*, 35:2540–2543, 1987.